Int J Earth Sciences (2001) 89 : 766–780
DOI 10.1007/s005310000106

ORIGINAL PAPER

Klaus Gessner · Sandra Piazolo · Talip Güngör
Uwe Ring · Alfred Kröner · Cees W. Passchier

Tectonic significance of deformation patterns in granitoid rocks of the Menderes nappes, Anatolide belt, southwest Turkey

Received: 5 May 1999 / Accepted: 29 March 2000 / Published online: 17 November 2000

Abstract Deformation fabrics in Proterozoic/Cambrian granitic rocks of the Çine nappe, and mid-Triassic granites of the Bozdag nappe constrain aspects of the tectonometamorphic evolution of the Menderes nappes of southwest Turkey. Based on intrusive contacts and structural criteria, the Proterozoic/Cambrian granitic rocks of the Çine nappe are subdivided into older orthogneisses and younger metagranites. The deformation history of the granitic rocks documents two major deformation events. An early, pre-Alpine deformation event (D_{PA}) during amphibolite-facies metamorphism affected only the orthogneisses and produced predominantly top-to-NE shear-sense indicators associated with a NE-trending stretching lineation. The younger metagranites are deformed both by isolated shear zones, and by a major shear zone along the southern boundary of the Çine submassif. We refer to this Alpine deformation event as D_{A3}. D_{A3} shear zones are associated with a N-trending stretching lineation, which formed during greenschist-facies metamorphism. Kinematic indicators associated with this stretching lineation reveal a top-to-south sense of shear. The greenschist-facies shear zones cut the amphibolite-facies structures in the orthogneisses. $^{207}Pb/^{206}Pb$ dating of magmatic zircons from a metagranite, which crosscuts orthogneiss containing amphibolite-facies top-to-NE shear-sense indicators, shows that D_{PA} occurred before 547.2±1.0 Ma. Such an age is corroborated by the observation that mid-Triassic granites of the Çine and Bozdag nappes lack D_{PA} structures. The younger, top-to-south fabrics formed most likely as a result of top-to-south Alpine nappe stacking during the collision of the Sakarya continent with Anatolia in the Eocene.

Keywords Multistage deformation · Granites · Mylonites · Zircon dating · Western Turkey · Eastern Mediterranean

K. Gessner (✉) · S. Piazolo · U. Ring · A. Kröner
C. W. Passchier
Institut für Geowissenschaften, Becherweg 21,
Johannes Gutenberg-Universität, 55099 Mainz, Germany
E-mail: gessk000@mail.uni-mainz.de

T. Güngör
Jeoloji Mühendisliği Bölümü, Dokuz Eylül Üniversitesi,
35100 Bornova (İzmir), Turkey

Introduction

During the past decade, tectonic studies in the Anatolide belt of southwest Turkey have focussed on late Alpine N/S-oriented extensional deformation, which accomplished part of the exhumation of the Menderes nappes (Sengör 1987; Hetzel and Ring 1993; Bozkurt and Park 1994, 1997a, 1997b; Hetzel et al. 1995a, 1995b; Verge 1995; Hetzel and Reischmann 1996; Emre and Sözbilir 1997; Isik and Tekeli, this volume). Structures that predate late-orogenic extension (e.g. Lackmann 1997; Collins and Robertson 1998; Gessner et al. 1998; Hetzel et al. 1998; Partzsch et al. 1998; Ring et al. 1999a) suggest a complex history of crustal shortening, the timing of which is largely unknown. Lackmann (1997), Gessner et al. (1998) and Hetzel et al. (1998) have stressed the regional importance of top-to-NE kinematic indicators in the central part of the Menderes nappes and attributed them to early Tertiary nappe stacking. Nevertheless, this interpretation is in contrast to existing regional tectonic models (Sengör and Yilmaz 1981; Sengör et al. 1984; Collins and Robertson 1998). Sengör et al. (1984) argued that the Menderes nappes had been deformed and metamorphosed during the Early Tertiary collision of the Sakarya continent with Anatolia (Gessner 2000). Sengör et al. (1984) interpreted the Menderes nappes to lie in the footwall of the southward-propagating Lycian nappes. The Lycian nappes consist of carbonate platform sediments of Neotethys, which are situated tectonically beneath ophiolitic rocks. The Lycian

Table 1 Age data of granitic rocks from the Menderes nappes

Lithology; locality	Age [Ma]	Method	Authors
Metagranites and orthogneisses; entire Anatolide belt	2555–1740	$^{207}Pb/^{206}Pb$ single zircon evaporation	Reischmann et al. (1991)
Birgi metagranite; Ödemis submassif	551±1.4	U-Pb dating	Hetzel et al. (1998)
Metagranite in Selimiye shear zone, southern Çine submassif	546.2±1.2	$^{207}Pb/^{206}Pb$ single zircon evaporation	Hetzel and Reischmann (1996)
Metagranites and orthogneisses; Çine nappe	541.4±2.5 to 528±4.3	$^{207}Pb/^{206}Pb$ single zircon evaporation	Dannat (1997)
Metagranites and Orthogneisses; southern Çine submassif	659±7; 563±3–521±8	$^{207}Pb/^{206}Pb$ single zircon evaporation, U-Pb dating	Loos and Reischmann (1999)
Granites in Bozdag nappe; Ödemis submassif	~240–250	^{207}Pb-^{206}Pb single zircon evaporation	Koralay et al. (1998)
Granites in Bozdag nappe; Ödemis submassif	240.3±2.2; 226.5±6.8	^{207}Pb-^{206}Pb single zircon evaporation	Dannat (1997)
Egrigöz granite; Gördes submassif	~20	U-Pb dating	Reischmann et al. (1991)
Salihli granodiorite; Ödemis submassif	19.5±1.4	$^{40}Ar/^{39}Ar$ – amphibole isochron age	Hetzel et al. (1995a)
Turgutlu and Salihli granodiorites; Ödemis submassif	13.1±0.2 to 12.2±0.4	$^{40}Ar/^{39}Ar$ – biotite isochron age	Hetzel et al. (1995a)

nappes are interpreted to root in the Izmir–Ankara suture zone to the north of the Menderes nappes (Collins and Robertson 1997). Collins and Robertson (1998) defined the Lycian nappes as a large-scale, thin-skinned thrust system and showed that within the Lycian nappes, polyphase, top-to-south thrust-sheet translation at upper crustal levels occurred from the Late Cretaceous to the Early Miocene. Following Sengör et al. (1984) and Collins and Robertson (1998), any major tectonic event related to Tertiary crustal convergence in the Menderes nappes should be characterised by top-to-south shearing.

As an attempt to reconcile the regional model of Sengör et al. (1984) with field evidence, we describe a sequence of deformation structures in orthogneisses and metagranites from the central and southern Menderes nappes. We have found these rocks especially suitable for distinguishing pre-Alpine from Alpine tectonic events because their age is well constrained by radiometric dating (Table 1; Hetzel and Reischmann 1996; Dannat 1997; Loos and Reischmann 1999). We interpret the deformation fabrics by suggesting a chronology of tectonometamorphic events and their corresponding kinematics.

Geological setting

Numerous late Tertiary to Recent graben divide the Anatolide belt of southwest Turkey into three geographically defined blocks (Sengör 1987), the so-called submassifs: the northern or Gördes submassif; the central or Ödemis submassif; and the southern or Çine submassif. In this study we focus on the latter two submassifs (Fig. 1).

Architecture of the Anatolide belt in southwest Turkey

Traditionally the Anatolide belt of southwest Turkey, or Menderes Massif, has been interpreted as the eastern lateral continuation of the Cycladic zone or Cycladic Massif. Dürr et al. (1978) based their regional-scale correlation on lithostratigraphic comparisons, proposing that an old crystalline core is overlain by Paleozoic and Mesozoic cover series with metamorphic grade decreasing up section in both the Anatolide belt and the Cycladic zone. This long-standing view has been challenged by recent geochronological studies, which show marked differences in the age of the basement of the Anatolide belt and the Cycladic zone, respectively, indicating that the basement of the Cycladic zone and the Anatolide belt cannot be correlated. Ring et al. (1999a) and Gessner (2000) proposed that two different units, the Cycladic blueschist unit (the middle unit in Fig. 1a) and the underlying Menderes nappes, make up the Anatolide belt.

In the Menderes nappes, pronounced magmatic activity occurred at the Proterozoic/Cambrian boundary (Hetzel and Reischmann 1996; Dannat 1997; Loos and Reischmann 1999). Minor magmatic events took place in the mid-Triassic (Dannat 1997; Koralay et al. 1998) and the Miocene (Hetzel et al. 1995a). In the Cycladic zone, the granitic basement is of Carboniferous age (Reischmann 1997; Engel and Reischmann 1998). In addition, there are Triassic intrusions (Reischmann 1997; Ring et al. 1999b) and prominent Miocene to recent magmatic activity in the Cycladic zone (e.g. Altherr et al. 1982; Robertson and Dixon 1984). Ring et al. (1999a) and Gessner 2000 supplied further evidence for major differences between the Anatolide belt and the Cycladic zone by showing that only the upper parts of the Anatolide belt can be correlated with the Cycladic zone. Ring et al. (1999a) proposed a subdivision of the Anatolide belt into three major tectonic units (Fig. 1): (a) the Izmir–An-

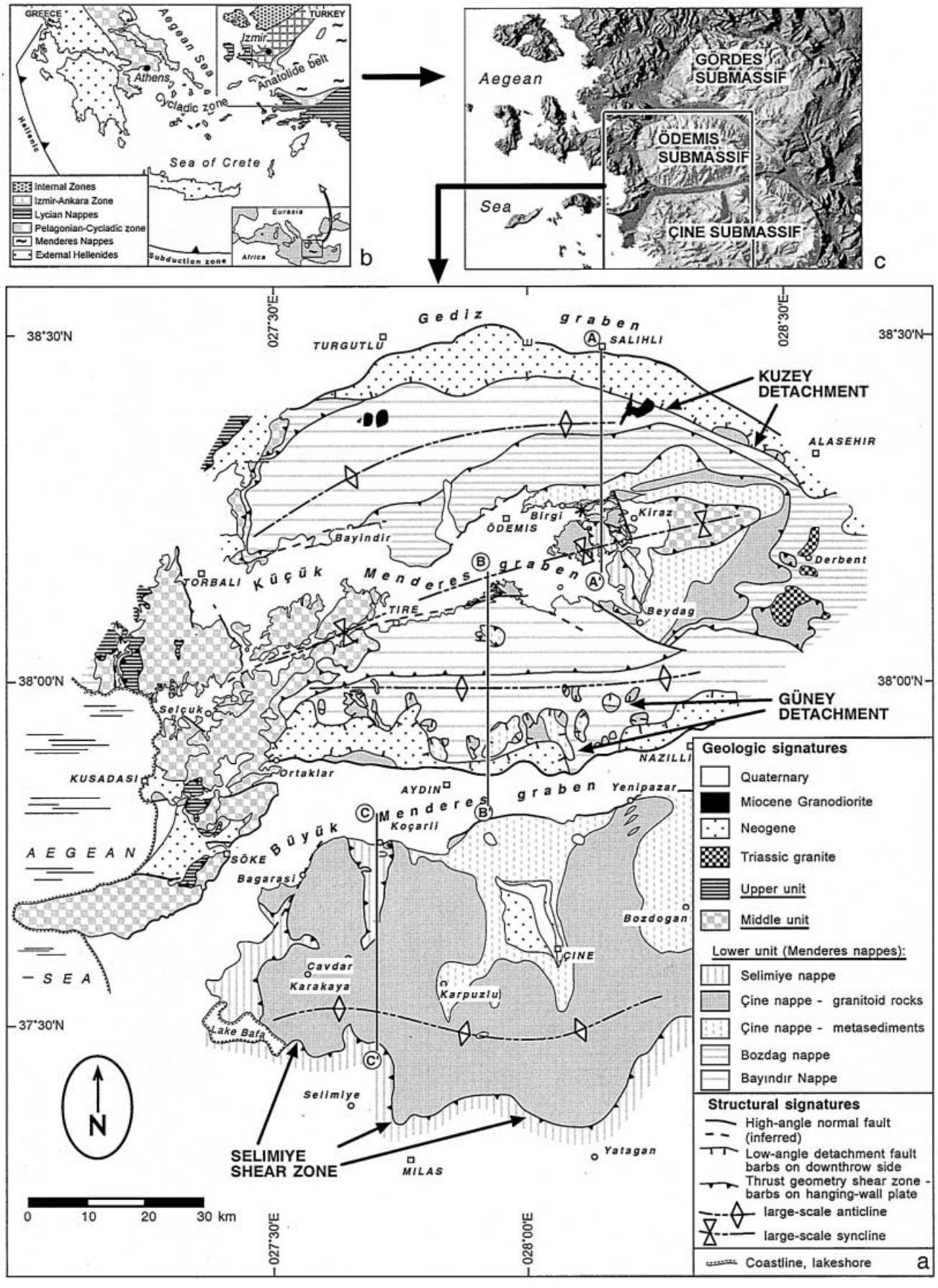
GREECE
TURKEY
Aegean Sea
Izmir
Athens
Anatolide belt
Cycladic zone
Hellenic
Sea of Crete
Internal Zones
Izmir-Ankara Zone
Lycian Nappes
Pelagonian-Cycladic zone
Menderes Nappes
External Hellenides
Eurasia
Africa
Subduction zone
b
Aegean
Sea
GÖRDES SUBMASSIF
ÖDEMIS SUBMASSIF
ÇINE SUBMASSIF
c
Gediz graben
TURGUTLU
SALIHLI
KUZEY DETACHMENT
ALASEHIR
Birgi
ÖDEMIS
Kiraz
Bayındır
Derbent
TORBALI
Küçük Menderes graben
TIRE
Beydag
GÜNEY DETACHMENT
Selçuk
NAZILLI
KUSADASI
Ortaklar
AYDIN
Yenipazar
Büyük Menderes graben
Koçarli
AEGEAN
SÖKE
Bagarasi
Bozdogan
ÇINE
Cavdar
Karakaya
Karpuzlu
SEA
Lake Bafa
Selimiye
SELIMIYE SHEAR ZONE
Yatagan
MILAS
N
0 10 20 30 km
38°30'N
38°00'N
37°30'N
027°30'E
028°00'E
Geologic signatures
Quaternary
Miocene Granodiorite
Neogene
Triassic granite
Upper unit
Middle unit
Lower unit (Menderes nappes):
Selimiye nappe
Çine nappe - granitoid rocks
Çine nappe - metasediments
Bozdag nappe
Bayındır Nappe
Structural signatures
High-angle normal fault (inferred)
Low-angle detachment fault barbs on downthrow side
Thrust geometry shear zone - barbs on hanging-wall plate
large-scale anticline
large-scale syncline
Coastline, lakeshore
a

Fig. 1 **a** Geological map of the Anatolide belt of southwest Turkey based on Scotford (1969), Güngör (1998), Hetzel et al. (1998), Candan and Dora (1998) and own observations. **b** Generalised tectonic map of the Aegean and adjacent mainlands showing major tectonic units, present-day Hellenic subduction zone and location of main map. **c** The alternation of narrow E/W-trending graben and mountain ranges resulting from neotectonic block faulting within the western Anatolian extensional province (Sengör 1987; Hancock and Barka 1987; Cohen et al. 1995). As a consequence, three grabens cut the metamorphic complex in the area, the Gediz graben to the north, the Küçük Menderes graben cutting the Ödemis submassif and the Büyük Menderes graben separating the Ödemis submassif from the Çine submassif

kara Zone and the Lycian nappes form the upper unit; (b) the Dilek nappe and the Selçuk melange form the middle unit (upper and middle units can be correlated with tectonic units in the Cycladic zone); and (c) the lower unit, referred to as the Menderes nappes, consists in ascending order of a lower metasedimentary succession, the Bayındır nappe, a metapelitic succession with abundant amphibolite and few marble lenses named the Bozdag nappe, a Proterozoic/Cambrian basement succession named the Çine nappe and an upper metasedimentary succession of intercalated marble and calcschist, the Selimiye nappe. The Menderes nappes have no counterpart in the adjacent Aegean region.

According to this subdivision the structurally lowest unit exposed in the Menderes nappes, the Bayındır nappe, is deformed only by one major Alpine tectonometamorphic event, whereas in the overlying Bozdag, Çine and Selimiye nappes pre-Alpine and Alpine events are documented. The subdivision of Ring et al. (1999a) is used in this study and illustrated in Figs. 1 and 2.

Tectonic contacts within the Menderes nappes

Tertiary greenschist-facies shear zones separate individual nappes within the Menderes nappes (Figs. 1, 2). The contact of the Bayındır nappe and the Bozdag is be described in Gessner 2000. The few good outcrops along this contact are characterised by chlorite-bearing phyllitic to phyllonitic lithologies with complex refolded fabrics. K. Gessner et al. (submitted) inferred a top-to-south sense of shear. The shear-sense indicators are overgrown by albite porphyroblasts, which commonly obscure mylonitic fabrics.

Within the Bozdag nappe, a penetrative foliation and a NE-trending stretching lineation formed under prograde amphibolite-facies metamorphic conditions (Lackmann 1997; Gessner et al. 1998; Ring et al. in press). Kinematic indicators associated with this stretching lineation show a top-to-NE sense of shear (Hetzel et al. 1998). The amphibolite-facies fabrics are cut by isolated shear zones, which formed under greenschist-facies metamorphic conditions (Hetzel et al. 1998). These shear zones produced a shear-band foliation and a north-trending stretching lineation. Associated with this stretching lineation are asymmetrical fabric elements indicating a top-to-south sense of shear. The retrograde fabrics dominate over the prograde fabrics towards the contact between the Bozdag nappe and the overlying Çine nappe. In the Derbent area, this contact is characterised by asymmetrical greenschist-facies top-to-south shear-band foliations in the Çine and Bozdag nappes. In the Bozdag nappe in the vicinity of the nappe contact with the Çine nappe, no relics of the previous amphibolite-facies fabric are preserved. In contrast, an early amphibolite-facies schistosity is preserved in orthogneisses within the Çine nappe. A mid-Triassic granite in the Derbent area (Fig. 1a) shows a stitching relationship with the nappe contact between the Bozdag and Çine nappes. Overall, the data suggest that the Bozdag/Çine nappe were part of a nappe stack that formed before the intrusion of the mid-Triassic granite and was reworked during Tertiary greenschist-facies deformation.

The Selimiye nappe tectonically overlies the Çine nappe in the central and southern submassifs (Figs. 1, 2). This is well documented along the southern margin of the Çine submassif where a large-scale south-dipping shear zone of pre-Late Eocene age (Hetzel and Reischmann 1996), hereafter named "Selimiye shear zone" is exposed. In the Selimiye shear zone, asymmetrical structures indicate a top-to-south sense of shear (Hetzel and Ring 1993; Bozkurt and Park 1994; Hetzel and Reischmann 1996). Within the Selimiye nappe, Bozkurt (1996) reported relics of a previous deformation event, which was characterised by a top-to-NE sense of shear. Bozkurt and Park (1994) and Hetzel and Reischmann (1996) interpreted the Selimiye shear zone as a crustal-scale extensional shear zone, whereas Collins and Robertson (1998) and Ring et al. (1999a) argued that the Selimiye shear zone is a thrust.

Bivergent extensional detachments

Southeast of Salihli and north of Aydın, isolated klippen of the Çine nappe occur in the hangingwall of two low-angle normal-fault systems related to late-orogenic extension (Fig. 1). These fault systems are exposed at the northern and southern margins of the Ödemis submassif and are termed Kuzey detachment and Güney detachment by Ring et al. (1999a).

The Kuzey detachment forms the northern slope of the Ödemis submassif where it is cut by normal faults bounding the Gediz graben. The Kuzey detachment is a large-scale top-to-north cataclastic shear zone with a dip of approximately 15°N (Fig. 2; Hetzel et al. 1995a). Orthogneisses of the Çine nappe and Miocene alluvial sediments occur in the hangingwall of the detachment.

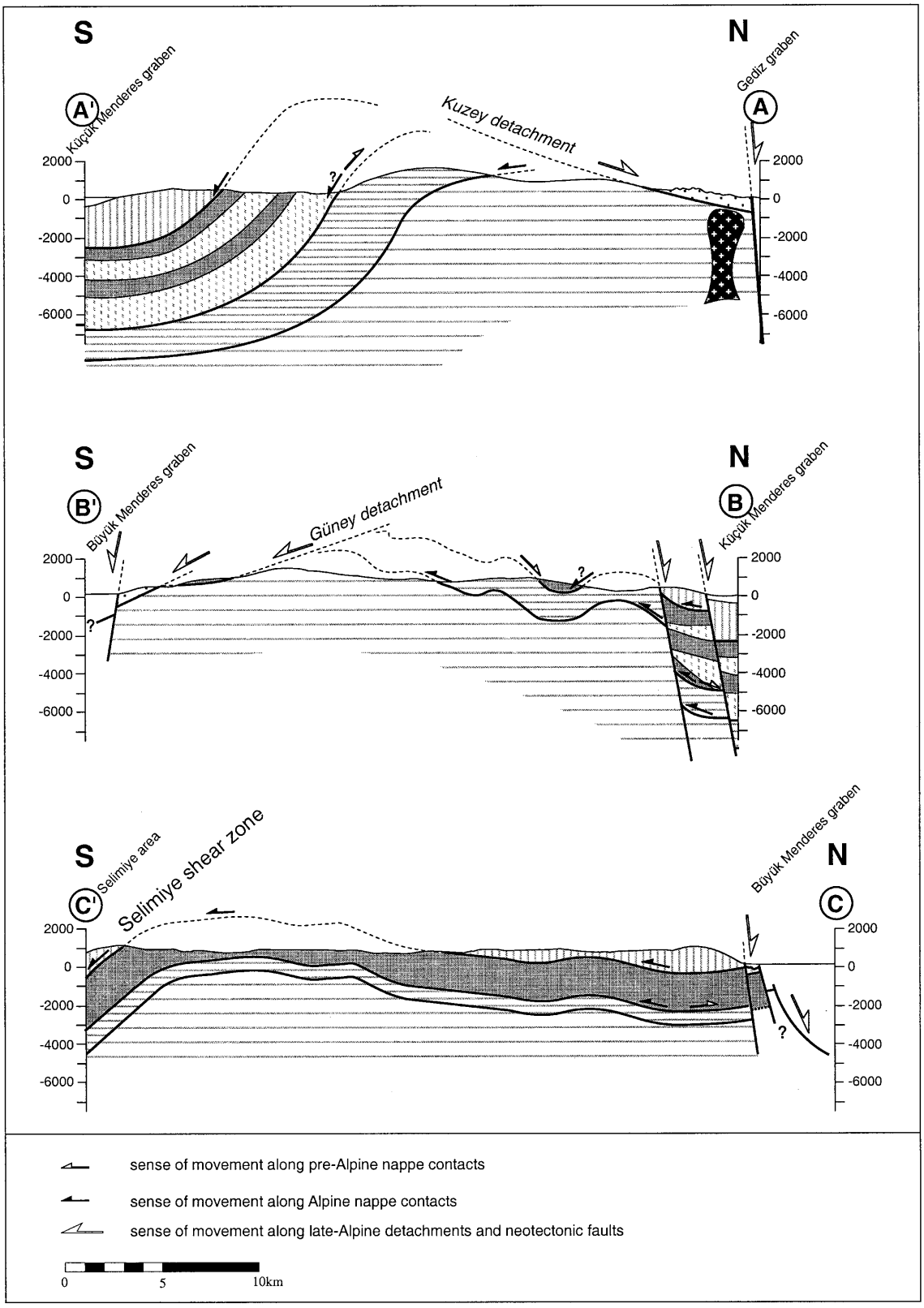

Fig. 2 Geological cross sections along section lines *A–A'*, *B–B'* and *C–C'* as illustrated in Fig. 1. Projection of foliation planes and fold axes into the section plane and extrapolation of large-scale surface structures to greater depths enhance the geometric viability; fill patterns are explained in Fig. 1

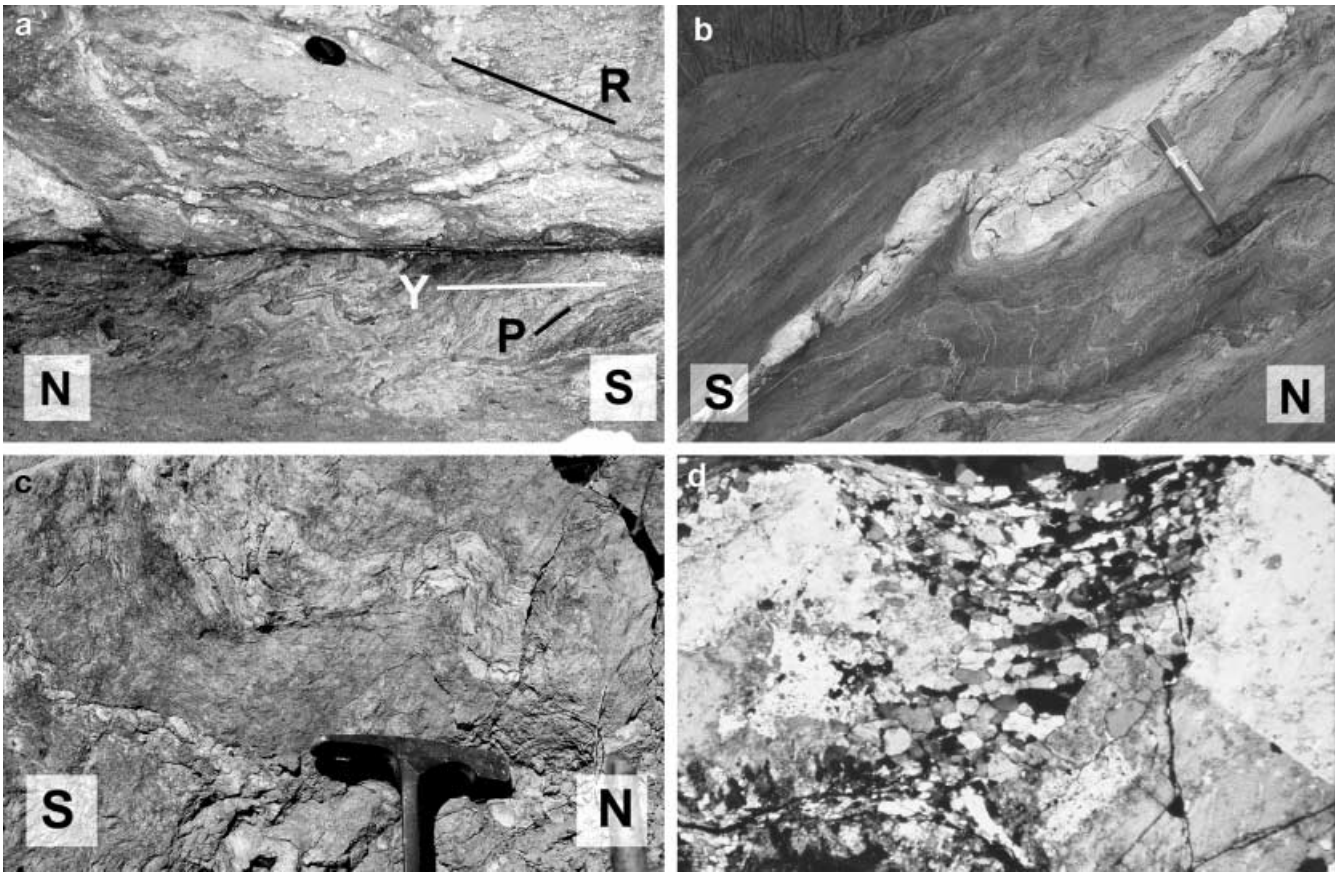

Fig. 3 **a** Cataclastic shear zone at the base of the Güney detachment system NW of Aydın. In the outcrop both the hangingwall rock unit, consisting of orthogneisses, and the phyllitic mica schist of the Bayındır nappe in the footwall show pronounced brittle deformation. A metre-thick zone of asymmetrically folded cataclasite (*lower part*) is cut by a discrete centimetre-thick gouge zone. The brittle shear plane fabrics in the orthogneiss represent a composite planar fabric (cf. Chester and Logan 1987; Cowan and Brandon 1994), where the gouge zone represents the Y plane parallel to the shear-zone boundaries. There is also a set of south-dipping synthetic Riedel or R planes. The shear sense is top to south. Location of outcrop: 37°57′48 N; 27°40′39 E. **b** Deformed intrusive contact between granite and sillimanite-bearing metapelite of the Çine nappe at the northeastern shore of Lake Bafa. Location of outcrop: 37°29′27 N; 27°32′13 E. **c** Folded vein of mid-Triassic granite in mica schist of the Bozdag nappe approximately 5 km southwest of Derbent. **d** Microphotograph of boudinaged potassium feldspar porphyroclast with recrystallised grains of smaller grain size forming the boudin neck. Field of view is 16×11 mm. Location of outcrop: 38°07′03 N; 28°09′21 E

The Güney detachment is exposed in the southern Ödemis submassif and has been described by Emre and Sözbilir (1997). Between Nazilli and Ortaklar, the footwall of the Güney detachment is formed by micaschists and marbles of the Bayındır nappe. Only in a small area north of Ortaklar is the footwall of the detachment made up of micaschists, marbles and serpentinites of the Selçuk melange (Fig. 1a). Asymmetrical fabric elements, such as Riedel composite structures (Chester and Logan 1987; Cowan and Brandon 1994), yield slip vectors that indicate top-to-south displacement (Fig. 3a; cf. Emre and Sözbilir 1997). Top-to-south shear is corroborated by the northerly dip of the overlying sediments. A marked difference to the Kuzey detachment is the much larger outcrop area of Çine nappe metamorphics in the hangingwall of the shear zone, where they form the basement to nonconformably overlying Miocene sediments. Both the supra-detachment sediments and their basement are cut by numerous cataclasites and gouges, thereby deforming the upper plate of the detachment into an array of tilted and rotated blocks. In their present position, the brittle shear zones depict low-angle normal- and also thrust-fault geometries. The occurrence of conglomerate in a cataclastic fault zone northwest of Aydın implies that brittle deformation was post- or syn-tectonic with respect to the formation of the supra-detachment basins in the Neogene. These structures are cut by neotectonic high-angle normal faults bounding the Büyük Menderes graben (Cohen et al. 1995).

In the Çine submassif, there is no indication for detachment faulting. In contrast to the Ödemis submassif, the Neogene sediments covering the Çine submassif appear to be undisturbed.

Granitic rocks of the Menderes nappes

The age of granitic intrusions in the Menderes nappes has been constrained by various geochronological studies (Table 1; Reischmann et al. 1991; Hetzel et al. 1995a; Hetzel and Reischmann 1996; Dannat 1997; Hetzel et al. 1998; Loos and Reischmann 1999). The data show that Proterozoic/Cambrian magmatic activity occurred in two distinct pulses at 550–570 Ma and at approximately 530 Ma, respectively. The Proterozoic/Cambrian intrusives occur only in the Çine and the Selimiye nappe; they are referred to as the Proterozoic/Cambrian granitoids in the remainder of the paper. According to Dannat (1997), these granitoids are peraluminous, strongly differentiated S-type granodiorites, tonalites and diorites. A subdivision of the granitic rocks into orthogneisses and metagranites is proposed below.

Triassic granites occur in the eastern part of the Ödemis submassif and intrude rocks of the Çine and Bozdag nappes, respectively. The geochemistry of these granites classifies them also as highly differentiated, peraluminous granites (Dannat 1997). Furthermore, Miocene granites occur in the Ödemis and Gördes submassifs.

Intrusive contacts

In the Çine nappe, the Neoproterozoic/Cambrian granitoids show abundant intrusive contacts towards metapelitic and migmatic gneisses, and with quartzofeldspathic metasediments (Fig. 3b). Furthermore, intrusive relationships exist between different granitoid lithologies in the Çine nappe. Intrusive contacts between Proterozoic/Cambrian granitoids and garnet-bearing metapelite of the Selimiye nappe are known from the Lake Bafa area (Erdogan and Güngör 1992; Hetzel and Reischmann 1996).

The mid-Triassic granites show intrusive contacts with metapelites of the Bozdag nappe in the Derbent area (Fig. 3c). O. Candan (pers. commun. 1998) also reported intrusive contacts of the granites with orthogneisses of the Çine nappe. The Miocene granites of the Ödemis submassif intruded into the Bayındır nappe (Hetzel et al. 1995a).

Subdivision of the Neoproterozoic/Cambrian granitic rocks in the Çine nappe

Our subdivision of granitic rocks in the Çine nappe into "older" orthogneisses and "younger" metagranites is based on structural characteristics and on intrusion relations. Our discrimination between orthogneisses and metagranites represents a simplification of the overall appearance of the granitoid protoliths. The terms "orthogneiss" and "metagranite" are used in a categorical rather than a descriptive sense. The typical appearance of an orthogneiss in the Menderes nappes is that of a protomylonite to mylonite with "augen"-shaped feldspar porphyroclasts. However, due to heterogeneous deformation, some orthogneisses are only weakly deformed. Some of these orthogneisses have been dated at 570–550 Ma (Loos and Reischmann 1999). The metagranites, on the other hand, are, in general, much less deformed than the orthogneisses and only show localised weakly deformed zones, which formed during greenschist-facies metamorphism. As is shown herein, the orthogneisses and metapelites of the Çine nappe are, like the mica schists of the Bozdag nappe, deformed by two consecutive sets of deformation fabrics. In contrast, the metagranites characteristically show only the second set of structures.

Both sets of granitoids of the Çine nappe formed during a series of intrusion stages. This is documented in the field by intrusive contacts between granitoids or xenoliths of earlier granitoids into later ones. It is beyond the scope of this study to resolve the number of intrusive stages within the granitoids, but it is important to note that the metagranites do not show the early structures and in places intruded the orthogneisses.

Deformation of the Neoproterozoic/Cambrian granitoids

It is possible to distinguish structures which formed during amphibolite-facies metamorphism from structures which formed under greenschist-facies conditions. This distinction is based on overprinting criteria and the different degree of metamorphism under which the structures formed. We can use the metamorphic criterion because the individual nappes do not show pronounced regional variations in metamorphic grade during a single metamorphic event. To constrain the metamorphic conditions during deformation, temperature-sensitive reaction textures within the foliation and the deformation behaviour of potassium feldspar has been used. Fabrics in which potassium feldspar dynamically recrystallised are likely to have been formed above 500 °C (Voll 1976; Tullis and Yund 1985, 1987, 1991).

The amphibolite-facies structures are associated with kinematic indicators, which show a dominantly top-to-NE shear sense, although there are regional variations in the sense of shear. We refer to this deformation as D_{PA} (where the suffix PA denotes pre-Alpine). The greenschist-facies event is referred to as the D_{A3} deformation (the suffix A3 denotes a third Alpine deformation event; note that D_{A1} and D_{A2} refer to high-pressure structures which occur exclusively in the middle unit). A more detailed description of the Alpine deformation history is given by Gessner

2000. Kinematic indicators of the greenschist-facies D_{A3} structures show a consistent top-to-south sense of shear.

Amphibolite-facies structures (D_{PA})

The orthogneisses have a protomylonitic to mylonitic foliation (S_{PA}) that consists of biotite and/or white mica. Magmatic potassium feldspar and plagioclase porphyroclasts are up to several centimetres in diameter and are deformed by dynamic recrystallisation of the outer rims forming core-and-mantle structures. Biotite grains are recrystallised with their [001]-planes oriented subparallel to S_{PA}. Less frequently, kinked relic grains of biotite with minor recrystallised rims exist with [001]-planes oriented at high angles to the foliation. In aluminium-rich orthogneisses, S_{PA} is formed by biotite that grows at the expense of millimetre- to centimetre-size garnets (Fig. 4a).

In S_{PA} a regionally consistent NE-trending stretching lineation (L_{PA}) is developed (Fig. 5a). Foliation and lineation form LS- or L-type tectonites. Elongated aggregates of recrystallised feldspar, quartz rods and elongated aggregates of recrystallised biotite grains form the stretching lineation. Recrystallised K-feldspar grains grew parallel to L_{PA} between boudinaged and displaced porphyroclasts (Fig. 3d). These recrystallised grains are tens to hundreds of microns in diameter.

Asymmetrical deformation fabrics useful for kinematic analysis are frequently developed in the orthogneisses. This includes asymmetrical recrystallised tails around feldspar porphyroclasts (sigma-type objects; sensu Passchier and Simpson 1986) and C- and C'-type shear bands (Berthé et al. 1979) at the decimetre scale. The kinematic interpretation of asymmetrical fabric elements (Passchier and Simpson 1986; Hanmer and Passchier 1991) reflects regional variations in shear sense (Fig. 6). North of the Büyük Menderes graben, top-to-NE shear-sense indicators (Fig. 4b) dominate. At the northwestern margin of the Çine submassif, symmetrical fabric elements, such as symmetrical strain shadows around feldspar and symmetrical foliation boudinage with "fish-mouth" quartz

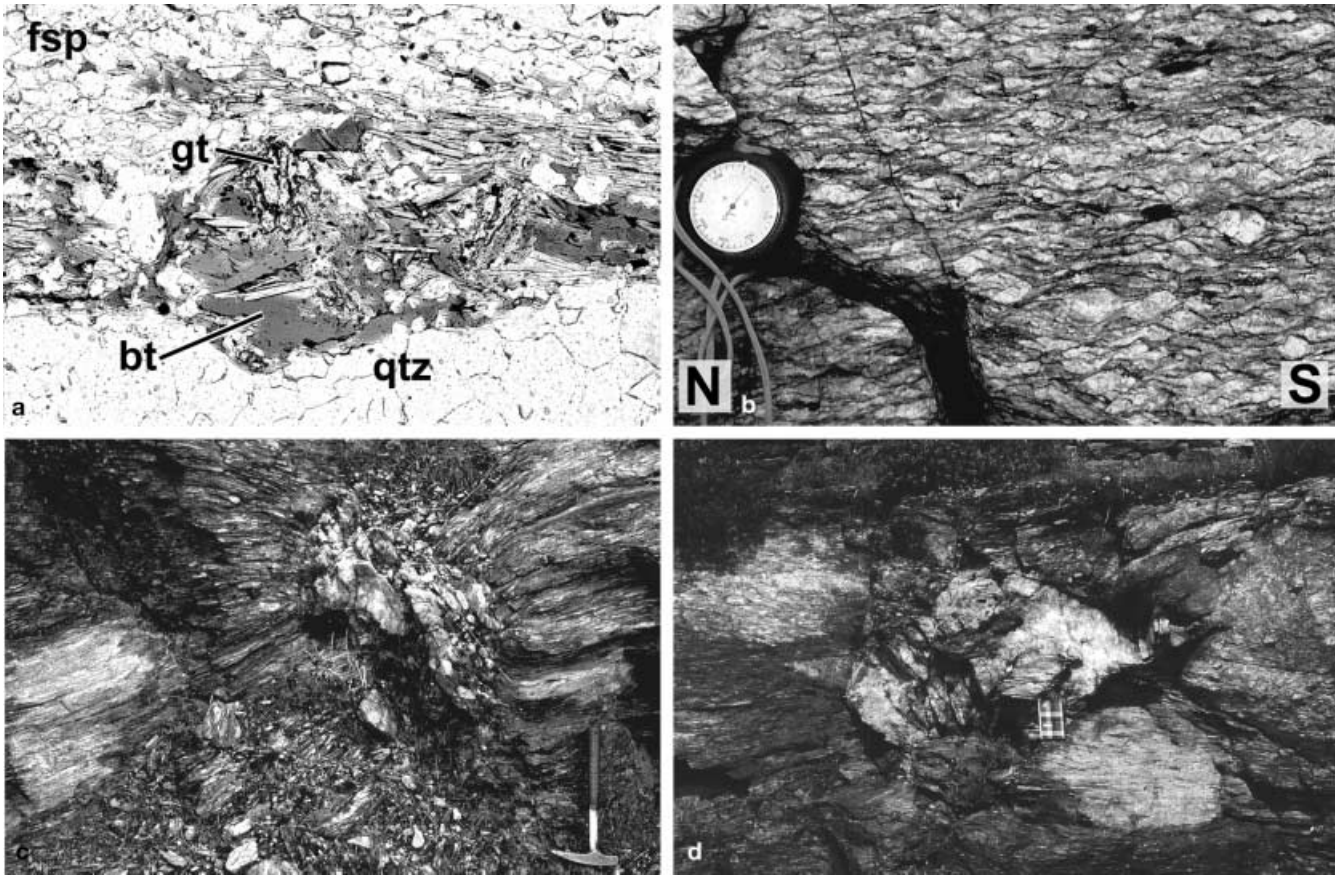

Fig. 4 **a** Photomicrograph of biotite grains growing at the expense of garnet in orthogneiss of the Çine nappe in the Ödemis submassif. The biotite grains mimic the shape of the resorbed garnet grain. Location of outcrop: 37°56′19 N; 28°00′47 E. *fsp* Feldspar; *bt* biotite; *gt* garnet; *qtz* quartz. **b** C'-type shear-band foliation (Berthé et al. 1979) indicating top-to-north sense of shear in orthogneiss of the Ödemis submassif. Note that the material in the strain shadows is mainly recrystallised potassium feldspar. Location of outcrop: 38°11′23 N; 28°03′57 E. **c** Foliation boudinage with quartz in the boudin neck. Symmetrical foliation boudinage is typical for the northwestern part of the Çine submassif. Location of outcrop: 37°39′33 N; 27°34′14 E. **d** Foliation boudinage in orthogneiss southeast of Bagarası with symmetric "fish-mouth"-type quartz pods in the neck of the boudin. Location of outcrop: 37°39′33 N; 27°34′14 E

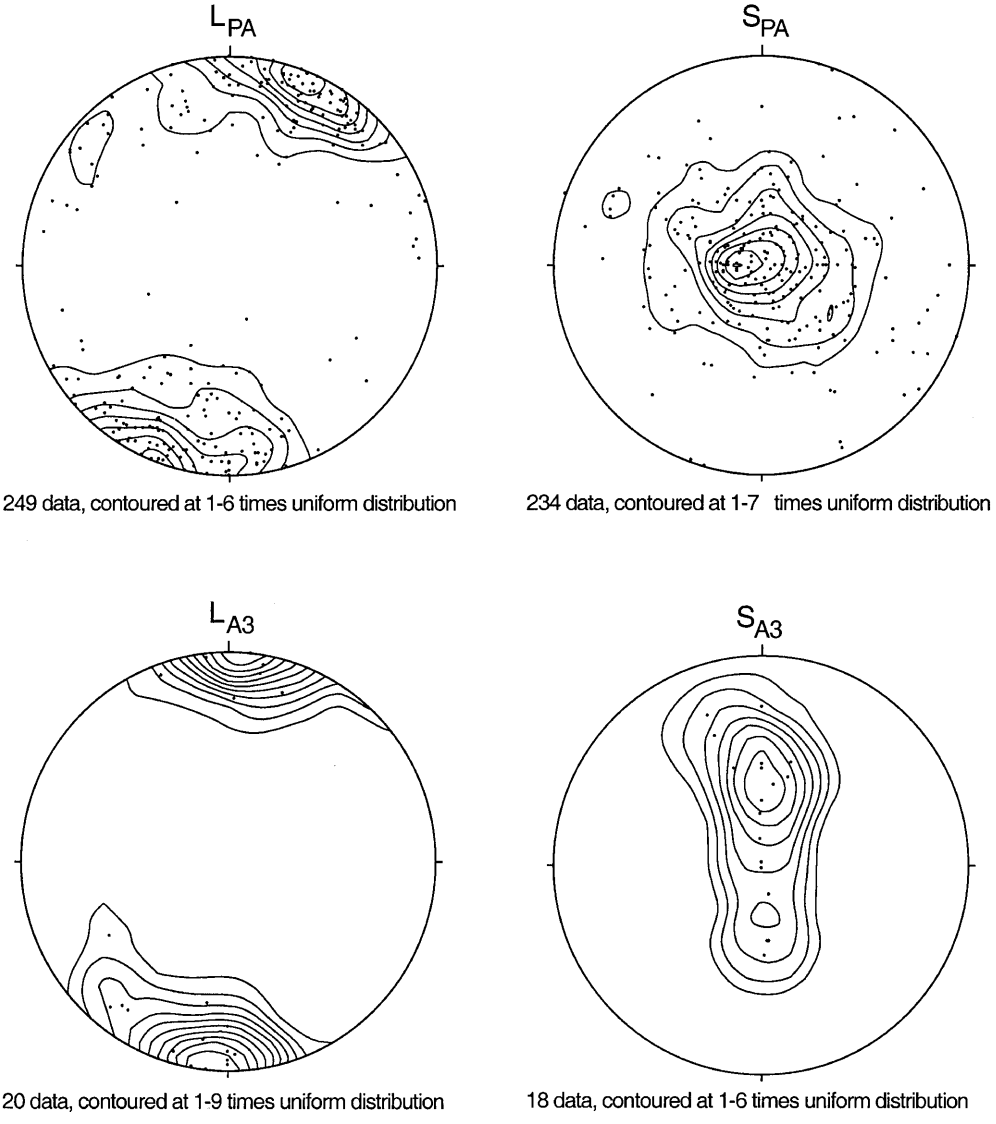

Fig. 5 Lower hemisphere equal-area projections of stretching lineations and associated foliation planes in granitic rocks of the Menderes nappes. *Upper row* Northeast-trending stretching lineations (L_{PA}) and foliation planes (S_{PA}) formed during amphibolite-facies metamorphism in orthogneisses of the Çine nappe. *Lower row* North-trending stretching lineations (L_{A3}) and foliation planes (S_{A3}) formed during greenschist-facies metamorphism in orthogneisses and metagranites of the Çine nappe

pods occur (Fig. 4c,d) together with minor top-to-NE kinematic indicators (Fig. 6). In the central Çine submassif, both top-to-NE and top-to-SW kinematic indicators have been mapped.

There is no evidence that the top-to-NE and top-to-SW kinematic indicators are of different generations, and no evidence that they developed during different metamorphic conditions. However, locally we observed that the top-to-SW indicators are inverted top-to-NE kinematic indicators due to later recumbent tight to isoclinal folding about axes parallel to the NE-trending D_{PA} stretching lineation.

Greenschist-facies structures (D_{A3})

Greenschist-facies deformation structures (D_{A3}) are the second set of fabrics in the orthogneisses, where they crosscut the amphibolite-facies D_{PA} structures, and are the only set of structures in the metagranites. In orthogneisses in the Çine and Ödemis submassifs, D_{PA} fabrics are locally cut by isolated, centimetre- to metre-thick, retrograde shear zones (Fig. 7; see also Hetzel et al. 1998). In these shear zones a new foliation (S_{A3}) formed. The development of S_{A3} is characterised by the breakdown of garnet, potassium feldspar and biotite, and the new growth of chlorite, albite and white mica. In S_{A3}, a N-trending stretching (L_{A3}) lineation formed and is expressed by stretched aggregates of quartz (Fig. 5b), chlorite and white mica.

In metagranites and orthogneisses of the Çine submassif, the greenschist-facies shear zones increase in number towards the Selimiye shear zone. In the Selimiye shear zone, the greenschist-facies structures obliterated all previous fabrics in the orthogneisses. Throughout the Selimiye shear zone, kinematic indicators provide a top-to-south sense of shear (Hetzel and Ring 1993; Bozkurt and Park 1994, 1997a, 1997b; Hetzel and Reischmann 1996). The formation of the

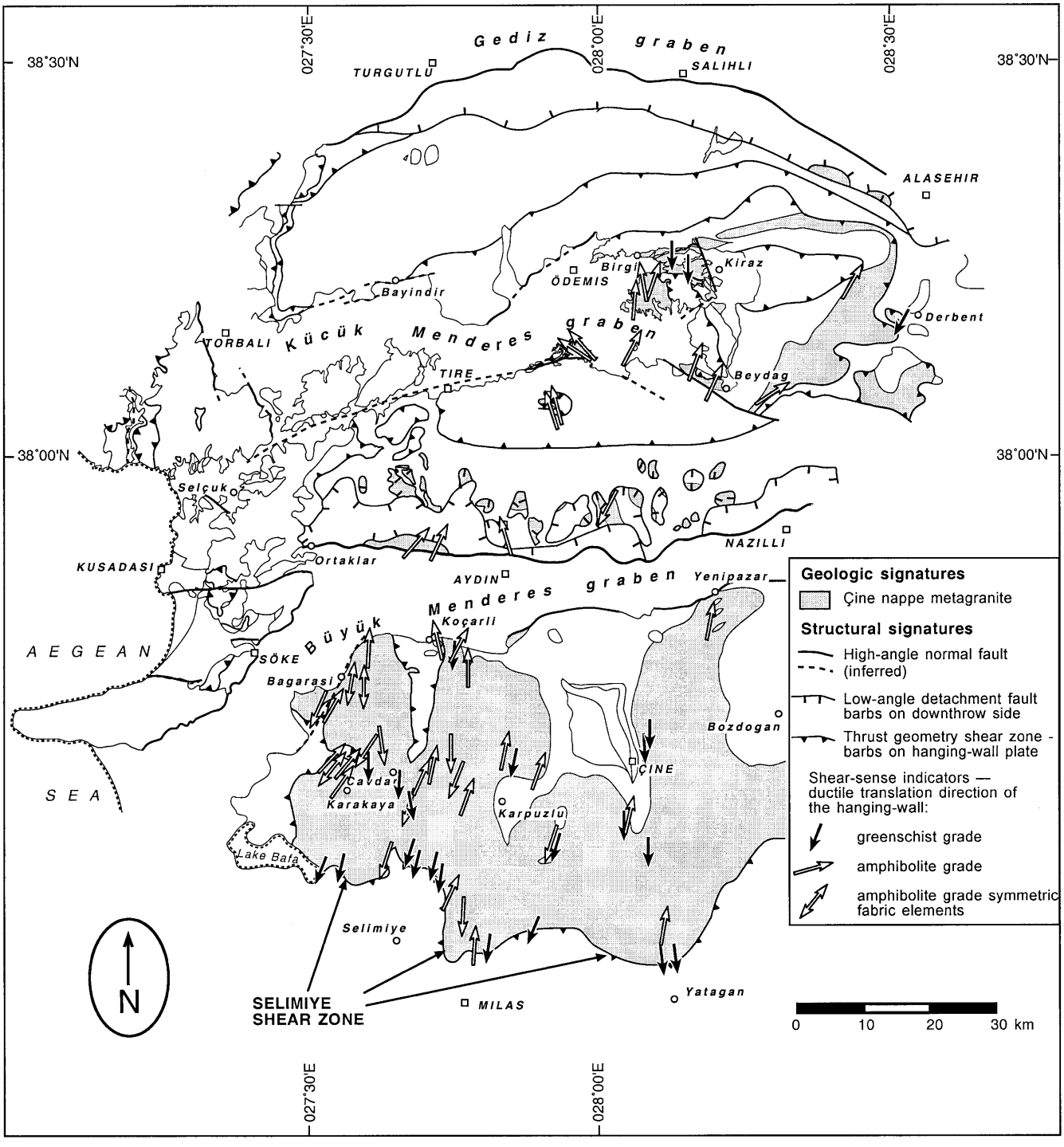

Fig. 6 Map shows D_{PA} (*white*) and D_{A3} (*black*) kinematic indicators in the Çine nappe granitoids. *Arrows* point to movement direction of the hangingwall

greenschist-facies structures probably took place at temperatures below 400–500 °C, because feldspar porphyroclasts and biotite are commonly not recrystallised but brittlely deformed (Fig. 8a; Bozkurt and Park 1997a).

In the footwall of the Selimiye shear zone, metagranites and orthogneisses locally display networks of ultracataclasites and pseudotachylites, which cut ductile greenschist-facies structures. In contrast, D_{A3} structures in the hangingwall of the Selimiye shear zone are ductile and available data suggests that the D_{A3} structures formed during prograde greenschist-facies metamorphism.

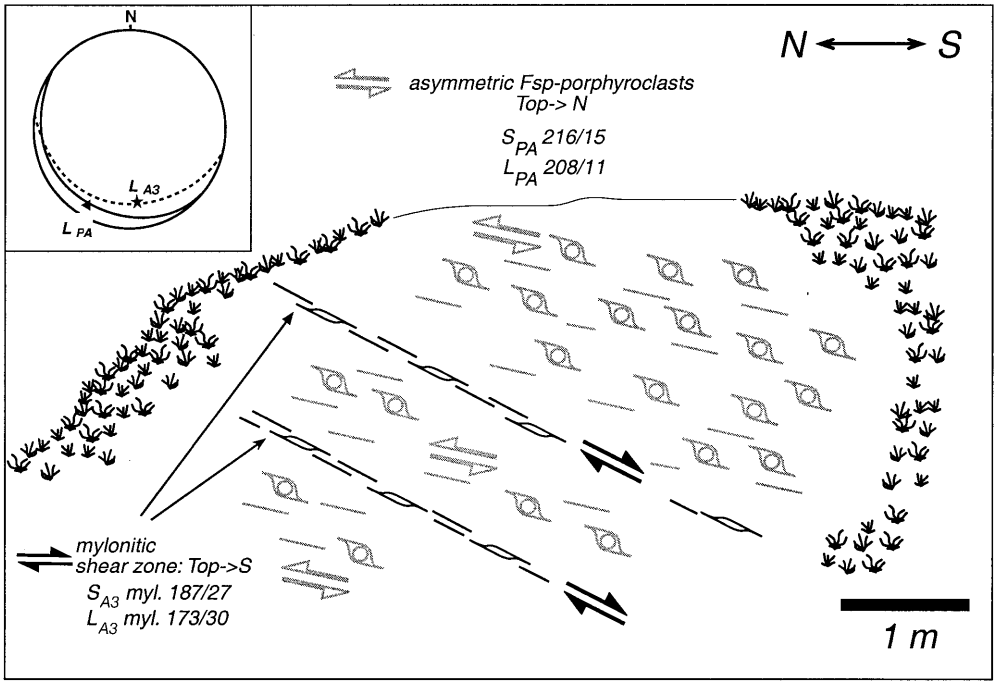

Fig. 7 Two sets of deformation fabrics in a road cut in the Çine submassif showing overprinting of pervasive amphibolite-facies structures, shown in *grey*, by localised greenschist-facies shear zones (shown in *black*). Location of outcrop: 37°43′70 N; 27°47′25 E

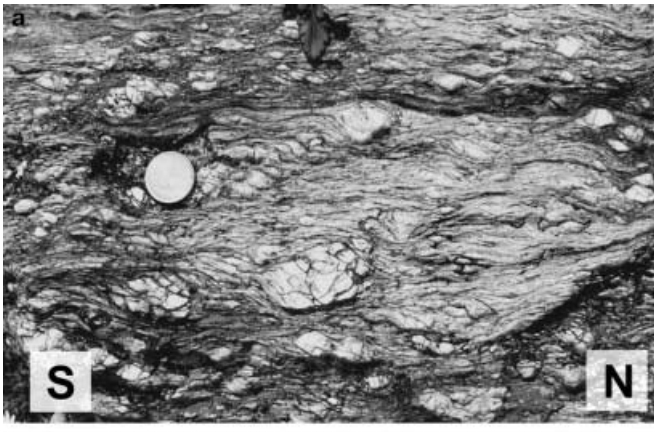

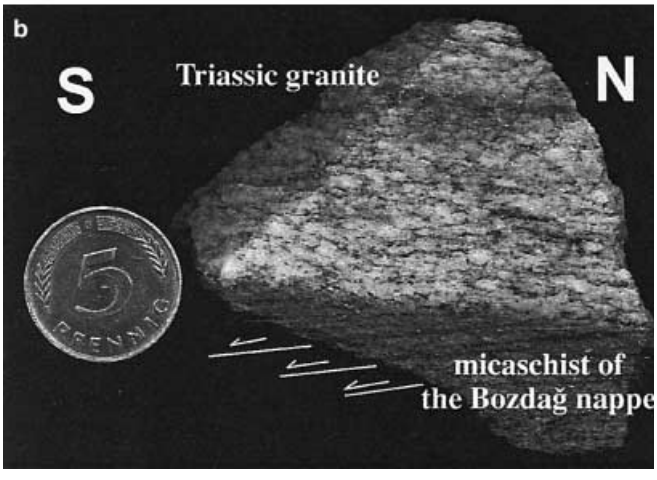

Fig. 8 a Greenschist-facies granitic mylonite with brittlely deformed mantled porphyroclasts of magmatic K-feldspar. Shear sense is top to south, as interpreted from clasts and shear bands. Note that the foliation has a steep southerly dip in the outcrop (180/72). Location of outcrop: 37°29′27 N; 27°32′13 E. **b** Polished section of the contact between the Mesozoic granite and the Bozdag nappe mica schist in a roadcut in Derbent. An asymmetrical shear-band cleavage, only developed in the mica schist, indicates top-to-south sense of shear, whereas in the granite only a weak fabric with σ-type porphyroclasts is visible

Deformation of the Triassic granites and their wallrocks

In the Triassic granites of the Derbent area (Fig. 1), white mica, flattened quartz and K-feldspar grains define a well-developed foliation. Biotite is rare; small poikiloblastic garnets, which are tens of microns in diameter, locally occur. Elongate quartz and feldspar grains and aligned white mica form a N-trending stretching lineation. Deformation fabrics in the granites are largely symmetrical; foliation boudinage is locally observed.

In the surrounding mica schists of the Bozdag nappe, granitic dikes are folded together with their wallrock. In these mica schists, a greenschist-facies foliation is associated with a N-trending stretching lineation. Foliation and stretching lineation are associated with millimetre-spaced shear-band cleavages formed by chlorite and biotite. Poikiloblastic garnets, which are tens of microns in size, are locally observed. The shear bands indicate a top-to-south sense of shear (Fig. 8b). In intercalated amphibolite lenses, a pre-

vious foliation is cut by biotite-bearing shear bands that also show a top-to-south sense of shear.

South of Derbent, the top-to-south fabrics in the micaschists of the Bozdag nappe can be followed across its upper nappe contact into the overlying Çine nappe. Asymmetrical shear bands indicating a top-to-south sense of shear overprint the D_{PA} fabrics in both the Çine and Bozdag nappes.

Granites crosscutting D_{PA} structures and their age

In a series of outcrops along a road from Eskiçine to Akçaova, a suite of metagranites intruded the orthogneisses. At the locality indicated in the legend of Fig. 9, a metagranite crosscuts an orthogneiss, which depicts well-developed D_{PA} structures. Because the intrusion age of the granite provides a minimum age for the D_{PA} structures in this part of the Çine submassif, we carried out $^{207}Pb/^{206}Pb$ dating on magmatic zircons from this metagranite by the zircon evaporation technique (Fig. 9).

The zircon evaporation technique has been described by Kober (1986, 1987). The method involves repeated evaporation and deposition of Pb isotopes from chemically untreated single grains in a double-filament arrangement (Kober 1987). The analytical procedures and instrumental conditions used in this study are detailed in Kröner and Hegner (1998). Repeated evaporation and deposition during the analytical procedure yielded $^{206}Pb/^{204}Pb$ ratios in excess of 40,000 with errors of 10% or less. Only zircons yielding such ratios were used for age assessment. Common lead was corrected, where necessary, using the model of Stacey and Kramers (1975).

No significant changes in the $^{207}Pb/^{206}Pb$ ratios were recorded on progressive heating, a feature suggesting that the zircons analysed contained only one stable radiogenic lead phase. The calculated ages and uncertainties are based on the means of all ratios evaluated. Mean ages and errors are presented as weighted means of the entire population (Table 2). The $^{207}Pb/^{206}Pb$ spectra are shown in a histogram, which permits visual assessment of the data distribution from which the ages are derived (Fig. 9b).

Since the evaporation technique only provides Pb isotopic ratios, there is no a priori way to determine whether a measured $^{207}Pb/^{206}Pb$ ratio reflects a concor-

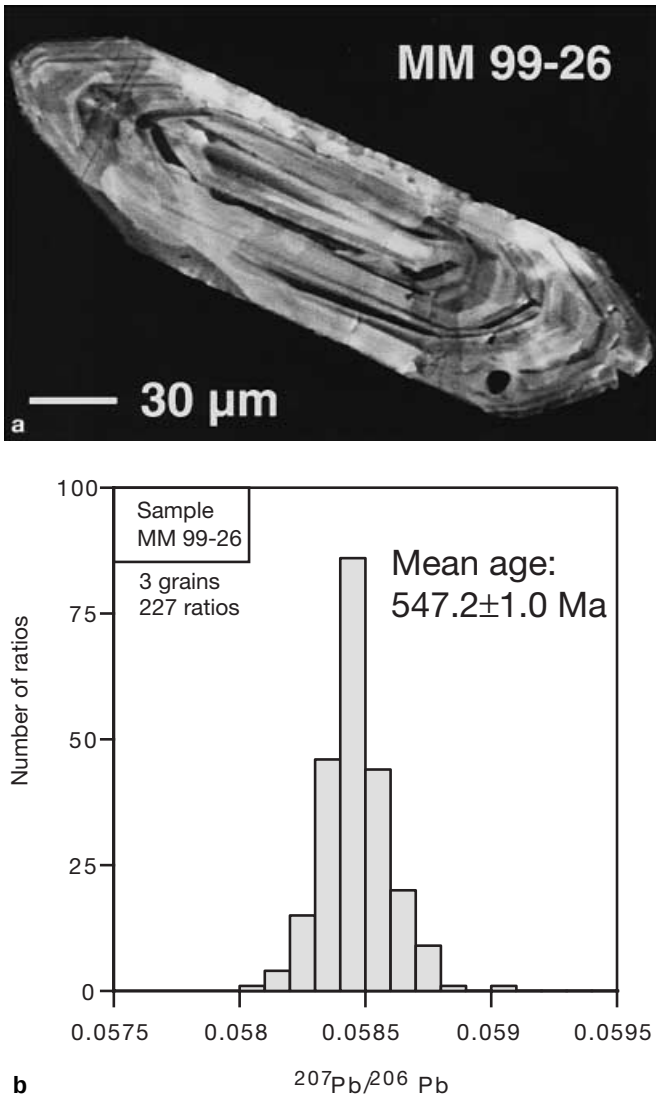

Fig. 9 **a** Cathodoluminiscence image of a typical long-prismatic igneous zircon from sample MM 99-26 used for $^{207}Pb/^{206}Pb$ dating. **b** Histogram showing the distribution of radiogenic Pb-isotope ratios derived from evaporation of zircons from metagranite sample MM 99-26 which crosscuts a mylonitically deformed orthogneiss in an outcrop SW of Çine on the road from Akçaova to Eskiçine (2.4 km west of turnoff from the Çine-Yatagan road). The spectrum plotted has been integrated from 227 ratios. Mean age is given with 2σ mean error

Table 2 Zircon morphology and Pb isotopic data from zircon evaporation

Sample	Zircon colour and morphology	Mass scans[a]	Evaporation temperature	Mean $^{207}Pb/^{206}Pb$ ratio and 2σ mean error	$^{207}/Pb/^{206}Pb$ age and 2σ m error[b]
MM 99-26	Clear, euhedral, long-prismatic	227	1595 °C	0.05846±0.0002	547.2±1.0[c]

[a] Number of $^{207}Pb/^{206}Pb$ ratios evaluated for age assessment
[b] Observed mean ratio corrected for non-radiogenic Pb; error based on uncertainties in counting statistics
[c] Error enhanced to reproducibility of internal standard (for details see Kröner and Hegner 1998)

dant age. Thus, principally, all $^{207}Pb/^{206}Pb$ ages determined by this method are necessarily minimum ages. Kröner and Hegner (1998) discussed this problem and provided reliability criteria for evaporation analyses. Comparative studies by single-grain evaporation, conventional U–Pb dating and ion-microprobe analysis have shown excellent agreement (Kröner et al. 1991; Cocherie et al. 1992; Jaeckel et al. 1997; Karabinos 1997).

The analysed metagranite contains clear, euhedral, long-prismatic zircons of typical igneous habit (Fig. 9a). Analysis of one fraction of three grains yielded a mean age of 547.2±1.0 Ma (Fig. 9) which we interpret as dating the time of protolith crystallisation. This age must be considered with caution since it is only one analysis, but it agrees well with zircon ages of other granitods within the area (cf. Table 1).

Discussion

A striking feature of the granitoid rocks throughout the Menderes nappes is the difference in composition and the nature of internal deformation. Ductile deformation fabrics vary according to their metamorphic grade and the type of shear zones in which they occur, and show overprinting relationships. The granitoids of the Çine and Bozdag nappe show two sets of ductile structures, which show consistent overprinting relationships and developed during different metamorphic conditions. The first set of structures (D_{PA}) formed during amphibolite-facies metamorphism and occur exclusively in orthogneisses of the Çine nappe and not in the metagranites and the mid-Triassic granites. One crosscutting metagranite yields a zircon age of 547.2± 1.0 Ma, which we interpret as an intrusion age. Orthogneisses dated at 550–570 Ma by Loos and Reischmann (1999) are deformed by D_{PA} structures. The consistent crosscutting relationships and our zircon dating of the crosscutting metagranite provides a robust and important time constraint demonstrating that D_{PA} is of late Neoproterozoic age.

D_{PA} fabrics with top-to-NE kinematics in orthogneisses and metapelites of the Çine nappe and micaschists and amphibolites of the Bozdag nappe in the Ödemis submassif are considered to result from a tectonic event that originally affected the Çine and Bozdag nappes. This is in accordance with the observation that D_{PA} structures can be traced across the nappe contact between the Çine and Bozdag nappes in the eastern Ödemis submassif.

An important feature seems to be the regional variation in kinematics of D_{PA} fabrics. In the Ödemis submassif, where the structurally lower parts of the Çine nappe are exposed, the D_{PA} kinematic indicators are consistently top-to-NE in the Bozdag nappe and in the overlying Çine nappe. In the Çine submassif, where structurally higher parts are exposed, symmetrical, top-to-SW and top-to-NE kinematic indicators have been mapped. Folding of top-to-NE fabrics with axes parallel to the stretching lineation, as locally observed, may be one reason for the local reversal in shear sense. However, the symmetrical fabrics still need an explanation. We envision that strongly non-coaxial deformation during D_{PA} was concentrated mainly at the base of the Çine nappe. In the middle and upper parts of the Çine nappe, the D_{PA} deformation is likely to have been close to coaxial, producing symmetrical fabrics and, at least in part, kinematic indicators with opposite kinematics.

A critical aspect of the tectonic interpretation of D_{PA} is the relation between D_{PA} deformation fabrics and metamorphism. In garnet-bearing orthogneisses in the higher parts of the Çine nappe in the Ödemis submassif, the D_{PA} structures formed during the breakdown of garnet to biotite, suggesting that D_{PA} occurred during retrograde amphibolite-facies conditions. However, Lackmann (1997 and Ring et al. (in press) showed that in metapelites of the basal Çine nappe and the directly underlying Bozdag nappe north of Birgi, prograde growth of garnet from biotite occurred synkinematically with the formation of the S_{PA} and L_{PA}. This suggests that D_{PA} occurred during prograde Barrovian metamorphism. The D_{PA} deformation juxtaposed the Çine and Bozdag nappes and both nappes show peak-metamorphic conditions of approximately 600–700 °C and 6–9 kbar (Lackmann 1997; Gessner et al. 1998). Because D_{PA} proceeded during prograde metamorphism in the metapelites of the Çine and Bozdag nappes, it is likely that D_{PA} fabrics formed during crustal thickening and resulted from horizontal crustal shortening. The discrepancy between the prograde and the retrograde fabrics may be explained by internal imbrication within the Çine nappe under higher-grade metamorphic conditions than those related to the emplacement of the Çine nappe on top of the Bozdag nappe. During nappe emplacement, reactivation of the tectonic contacts within the Çine nappe may have caused retrogression of the fabrics. Another explanation might be that the breakdown and growth of garnet occurred simultaneously under the same metamorphic conditions due to different bulk chemistries.

During the D_{A3} event, the granitoids of the Çine and Bozdag nappe were deformed heterogeneously by greenschist-facies metamorphism. D_{A3} caused regionally consistent top-to-south tectonic transport. Because D_{A3} affects the mid-Triassic granites, it is of post-mid-Triassic age. Our work in Cretaceous metasediments of the middle unit indicates that D_{A3} can also be mapped in these metasediments and must therefore be of Alpine age. Gessner 2000 argues that D_{A3} represents a complex deformation causing the assembly of the present nappe pile of the Anatolide belt in the Eocene.

Another important question is whether or not D_{A3} formed during an extensional or a contractional event. It has been shown that brittle–ductile and brittle

extensional structures formed during the late Alpine tectonic history of the Menderes nappes (cf. Hetzel et al. 1995a, 1995b; Hetzel et al. 1998; Emre and Sözbilir 1997). However, not all greenschist-facies shear zones are compatible with the bivergent orogenic extension model suggested by Hetzel et al. (1995b) and Hetzel et al. (1998). Collins and Robertson (1998), Ring et al. (1999a) and Gessner 2000 proposed that the D_{A3} Selimiye shear zone formed in response to crustal shortening. As noted by Hetzel and Reischmann (1996) and Collins and Robertson (1998), structure and metamorphic gradient of the Selimiye shear zone are in marked contrast to typical core-complex-type extensional detachments. Furthermore, deformation/metamorphism relationships indicate that D_{A3} structures formed during prograde greenschist-facies metamorphism or at the peak of the latter (Gessner 2000). Collectively, these observations suggest that D_{A3} is related to crustal shortening.

The widespread occurrence of rocks of the Çine nappe on top of the Bayındır nappe, especially north of Aydın, has been attributed to thrusting by Candan et al. (1992) and Lips (1998). In the Ödemis area, however, the Çine nappe occurs above the Bozdag nappe, which in turn rests upon the Bayındır nappe. This nappe pile, together with the overlying middle and upper units, was finally assembled during greenschist-facies metamorphism (Ring et al. 1999a; Gessner 2000). The contact between the Çine and Bayındır nappe north of Aydın is a cataclastic fault zone. The footwall of this fault zone is not always the Bayındır nappe; north of Ortaklar, the Selçuk melange is in the footwall of this cataclastic fault zone. These observations indicate that the cataclastic fault zone must be a relatively late, i.e. Miocene or Pliocene structure. Furthermore, there is no indication of thrusting or reverse faulting in the Neogene sediments. In accordance with Emre and Sözbilir (1997), we propose that the Güney detachment cut out the entire Bozdag nappe and placed the Çine nappe above the Bayındır nappe in this area.

Conclusion

Granitoids of the Çine and Bozdag nappes show two distinct sets of structures which formed during different orogenies. The first set of structures formed during amphibolite-facies metamorphism in the latest Proterozoic and caused, at least in part, internal imbrication in the Menderes nappes. During the Alpine orogeny, the second set of structures formed during greenschist-facies metamorphism. This second set of structures is attributed to horizontal crustal shortening and caused the final juxtaposition of the Menderes nappes with the overlying units of the Cycladic blueschist unit, the Izmir–Ankara suture zone and the Lycian nappes during collision of Anatolia with the Sarakaya continent to the north.

Acknowledgements This study was funded by the "Deutsche Forschungsgemeinschaft" (grants Ri 538/4-1, 4-2 and 4-3). We thank Andreas Möller for continuous support during processing of the zircons. We also thank G. Park and P. Gautier for reviews, and E. Bozkurt for editorial assistance.

References

Altherr R, Kreuzer H, Wendt I, Lenz H, Wagner GH, Keller J, Harre W, Höhndorf A (1982) A late Oligocene/early Miocene high temperature belt in the Attic-Cycladic crystalline complex (SE Pelagonian, Greece). Geol Jahrb E23:97–164

Berthé D, Choukroune P, Jegoutzo P (1979) Orthogneiss, mylonite and non-coaxial deformation of granites: the example of the South Armorican shear zone. J Struct Geol 1:31–42

Bozkurt E (1996) Metamorphism of Paleozoic schists in the southern Menderes Massif: field, petrographic, textural and microstructural evidence. Turk J Earth Sci 5:105–121

Bozkurt E, Park RG (1994) Southern Menderes Massif: an incipient metamorphic core complex in western Anatolia, Turkey. J Geol Soc Lond 151:213–216

Bozkurt E, Park RG (1997a) Microstructures of deformed grains in the augen gneisses of southern Menderes Massif (western Turkey) and their tectonic significance. Geol Rundsch 86:103–119

Bozkurt E, Park RG (1997b) Evolution of a mid-Tertiary extensional shear zone in the southern Menderes Massif, western Turkey. Bull Soc Géol France 168:3–14

Candan O, Dora OÖ (1998) The generalized geological map of the Menderes Massif. Jeol Mühendisligi Bölümü, Dokuz Eylül Univ, Izmir, Turkey

Candan O, Dora OÖ, Kun N, Akal C, Koralay E (1992) Aydýn Daglarý (Menderes Masifi) güney kesimindeki allokton metamorfik birimler (Allochtonous metamorphic units at the southern part of Aydýn Monutains, Menderes Massif). Bull Turk Assoc Pet Geol 4:93-110

Candan O, Dora OÖ, Dürr S, Oberhänsli R (1994) Erster Nachweis von Granulit- und Eklogit-Relikten im Menderes Massiv/Türkei. Göttinger Arb Geol Paläontol Sb1:217–220

Chester FM, Logan JM (1987) Composite planar fabric of gouge from the Punchbowl Fault, California. J Struct Geol 9:621–634

Cocherie A, Guerrot C, Rossi PH (1992) Single-zircon dating by step-wise Pb evaporation: comparison with other geochronological techniques applied to the Hercynian granites of Corsica, France. Chem Geol 101:131–141

Cohen HA, Dart CJ, Akyüz HS, Barka A (1995) Syn-rift sedimentation and structural development of the Gediz and Büyük Menderes graben, western Turkey. J Geol Soc Lond 152:629–638

Collins AS, Robertson AHF (1997) Lycian Melange, southwest Turkey: an emplaced Cretaceous accretionary complex. Geology 25:255–258

Collins AS, Robertson AHF (1998) Process of Late Cretaceous to Late Miocene episodic thrust-sheet translation in the Lycian Taurides. J Geol Soc Lond 155:759–772

Cowan DS, Brandon MT (1994) A symmetry-based method for kinematic analysis of large-slip brittle fault zones. Am J Sci 294:257–306

Dannat C (1997) Geochemie, Geochronologie und Nd- Sr-Isotopie der granitoiden Kerngneise des Menderes Massivs, SW-Türkei. PhD thesis, Johannes Gutenberg Univ, Mainz, pp 1–120

Dürr S, Altherr R, Keller J, Okrusch M, Seidel E (1978) The median Aegean crystalline belt: stratigraphy, structure, metamorphism, magmatism. In: Cloos H, Roeder D, Schmidt K (eds) Alps, Appeninnes, Hellenides. Schweizerbart, Stuttgart, pp 537–564

Emre T, Sözbilir H (1997) Field evidence for metamorphic core complex, detachment faulting and accommodation faults in the Gediz and Büyük Menderes grabens, western Anatolia. Proc IESCA 1:73–94

Engel M, Reischmann T (1998) Single zircon geochronology of orthogneisses from Paros, Greece. Bull Geol Soc Greece 32:91–99

Erdogan B, Güngör T (1992) Stratigraphy and tectonic evolution of the northern margin of the Menderes Massif. Bull Turk Assoc Petrol Geol 4:9–34

Gessner K (2000) Eocene nappe tectonics and late-Alpine extension in the central Anatolide belt, western Turkey – structure, kinematics and deformation history. PhD thesis, Univ. Mainz, Germany (URL: http://ArchiMed.uni-mainz.de/pub/2000/0062)

Gessner K, Güngör T, Ring U, Passchier CW (1998) Structure and crustal thickening of the Menderes massif, southwest Turkey, and consequences for large-scale correlations between Greece and Turkey. Bull Geol Soc Greece 32:145–152

Güngör T (1998) Stratigraphy and tectonic evolution of the Menderes Massif in the Söke-Selçuk region. PhD thesis, Dokuz Eylül Univ, Izmir, Turkey

Hancock PL, Barka AA (1987) Kinematic indicators on active normal faults in western Turkey. J Struct Geol 9:573–584

Hanmer S, Passchier CW (1991) Shear sense indicators: a review. Geol Surv Can Pap 90:1–71

Hetzel R, Reischmann T (1996) Intrusion age of Pan-African augen gneisses in the southern Menderes massif and the age of cooling after Alpine ductile extensional deformation. Geol Mag 133:565–572

Hetzel R, Ring U (1993) Extensional collapse of the Menderes Massif, western Turkey: preliminary data. Terra Nostra 1:18

Hetzel R, Ring U, Akal C, Troesch M (1995a) Miocene NNE-directed extensional unroofing in the Menderes massif, southwestern Turkey. J Geol Soc Lond 152:639–654

Hetzel R, Passchier CW, Ring U, Dora OÖ (1995b) Bivergent extension in orogenic belts: the Menderes massif, southwestern Turkey. Geology 23:455–458

Hetzel R, Romer RL, Candan O, Passchier CW (1998) Geology of the Bozdag area, central Menderes massif, SW-Turkey: Pan African basement and Alpine deformation. Geol Rundsch 87:394–380

Isik V, Tekeli O (2000) Late orogenic crustal extension in the northern Menderes massif (western Turkey): evidence for metamorphic core complex formation. Int J Earth Sci DOI 10.1007/s005310000105

Jaeckel P, Kröner A, Kamo SL, Brandl G, Wendt JI (1997) Late Archean to early Proterozoic granitoid magmatism and high-grade metamorphism in the central Limpopo belt, South Africa. J Geol Soc Lond 154:25–44

Karabinos P (1997) An evaluation of the single-grain zircon evaporation method in highly discordant samples. Geochim Cosmochim Acta 61:2467–2474

Kober B (1986) Whole grain evaporation for $^{207}Pb/^{206}Pb$-age investigations using a double-filament ion source. Contrib Mineral Petrol 93:482–490

Kober B (1987) Single-zircon evaporation combined with Pb^{+}-emitter bedding for $^{207}Pb/^{206}Pb$-age investigations using thermal ion mass spectroscopy, and implications to zirconology. Contrib Mineral Petrol 96:63–71

Koralay E, Satır M, Dora OÖ (1998) Geochchronologic evidence of Triassic and Precambrian magmatism in the Menderes Massif, west Turkey. Abstr 3rd Int Turk Geol Symp Ankara 1:285

Kröner A, Hegner E (1998) Geochemistry, single zircon ages and Sm-Nd systematics of granitoid rocks from the Gory Sowie (Owl Mountains), Polish West Sudetes: evidence for early Palaeozoic are-related plutonism. J Geol Soc Lond 155:711–724

Kröner A, Byerly CR, Lowe DR (1991) Chronology of early Archaean granite-greenstone evolution in the Barberton Mountain Land, South Africa, based on precise dating by single zircon evaporation. Earth Planet Sci Lett 103:41–54

Lackmann W (1997) P–T Entwicklung von Metapeliten des zentralen Menderes Massivs, Türkei. Diploma thesis, Johannes Gutenberg Univ, Mainz, 75 pp

Lips ALW (1998) Temporal constraints on the kinematics of the destabilization of an orogen; syn- to post-orogenic collapse of the northern Aegean region. Geol Ultraiectina 166:1–223

Loos S, Reischmann T (1999) The Evolution of the southern Menderes Massif in SW Turkey as revealed by Zircon dating. J Geol Soc Lond 156:1021–1030

Partzsch J, Oberhänsli R, Candan O, Warkus FC (1998) The evolution of the central Menderes Massif, west Turkey: a complex nappe pile recording 1.0 Ga of geological history. Freiberg Forschungsh C471:166–168

Passchier CW, Simpson C (1986) Porphyroclast systems as kinematic indicators. J Struct Geol 8:831–844

Reischmann T (1997) Single zircon Pb/Pb dating of tectonic units from the Metamorphic Complex of Naxos, Greece. Terra Nova 9:496

Reischmann T, Kröner A, Todt W, Dürr S, Sengör AMC (1991) Episodes of crustal growth in the Menderes Massif, W Turkey, inferred from Zircon dating. Terra Abstr 3:34

Ring U, Gessner K, Güngör T, Passchier CW (1999a) The Menderes Massif of western Turkey and the Cycladic Massif in the Aegean: Do they really correlate? J Geol Soc Lond 156:3–6

Ring U, Laws S, Bernet M (1999b) Structural analysis of a complex nappe sequence and late-orogenic basins from the Aegean Samos Island, Greece. J Struct Geol 21:1575–1601

Ring U, Willner AP, Lackmann W (in press) Stacking of nappes with different pressure-temperature paths: an example from the Menderes nappes of Western Turkey. Am J Sci

Robertson AHF, Dixon JE (1984) The geological evolution of the eastern Mediterranean. Geol Soc Lond Spec Publ 17:1–174

Scotford DM (1969) Metasomatic augen gneiss in greenschist facies, western Turkey. Bull Geol Soc Am 80:1079–1094

Sengör AMC (1987) Cross-faults and differential stretching of hanging walls in regions of low-angle normal faulting: examples from Western Turkey. In: Coward MP, Dewey SF, Hancock PL (eds) Continental Extensional Tectonics. Geol Soc Lond Spec Publ, 28:575–589

Sengör AMC, Yilmaz Y (1981) Tethyan evolution of Turkey: a plate tectonic approach. Tectonophysics 75:181–241

Sengör AMC, Satır M, Akkök R (1984) Timing of tectonic events in the Menderes Massif, western Turkey: implications for tectonic evolution and evidence for Pan-African basement in Turkey. Tectonics 3:693–707

Stacey JS, Kramers JD (1975) Approximation of terrestrial lead isotope evolution by a two-stage model. Earth Planet Sci Lett 26:207–221

Tullis J, Yund RA (1985) Dynamic recrystallisation of feldspar: a mechanism for ductile shear zone formation. Geology 13:238–241

Tullis J, Yund RA (1987) Transition from cataclastic flow to dislocation creep of feldspar: mechanisms and microstructures. Geology 15:606–609

Tullis J, Yund RA (1991) Diffusion creep in feldspar aggregates: experimental evidence. J Struct Geol 13:987–1000

Verge N (1995) Oligo-Miocene extensional exhumation of the Menderes Massif, western Anatolia. Terra Abstr 8:117

Voll G (1976) Recrystallisation of quartz, biotite and feldspars from Erstfeld to the Leventina nappe, Swiss Alps, and its geological significance. Schweiz Mineral Petrogr Mitt 56:641–647